Microstructure and Mechanical Properties of Ultrafine-Grained Al-6061 Prepared Using Intermittent Ultrasonic-Assisted Equal-Channel Angular Pressing

Jianxun Lu, Xiaoyu Wu, Zhaozhi Wu, Zhiyuan Liu, Dengji Guo, Yan Lou, and Shuangchen Ruan

Equal-channel angular pressing (ECAP) is an efficient technique to achieve grain refinement in a wide range of materials. However, the extrusion process requires an excessive extrusion force, the microstructure of ECAPed specimens scatters heterogeneously because of considerable fragmentation of the structure and strain heterogeneity, and the resultant ultrafine grains exhibit poor thermal stability. The intermittent ultrasonic-assisted ECAP (IU-ECAP) approach was proposed to address these issues. In this work, ECAP and IU-ECAP were applied to produce ultrafine-grained Al-6061 alloys, and the differences in their mechanical properties, microstructural characteristics, and thermal stability were investigated. Mechanical testing demonstrated that the necessary extrusion force for IU-ECAP was significantly reduced; even more, the microhardness and ultimate tensile strength were strengthened. In addition, the IU-ECAPed Al alloy exhibited a smaller grain size with a more homogeneous microstructure. X-ray diffraction analysis indicated that the intensities of the textures were weakened using IU-ECAP, and a more homogeneous microstructure and larger dislocation densities were obtained. Investigation of the thermal stability revealed that the ultrafine-grained materials produced using IU-ECAP recrystallized at higher temperature or after longer time; the materials thus exhibited improved thermal stability.
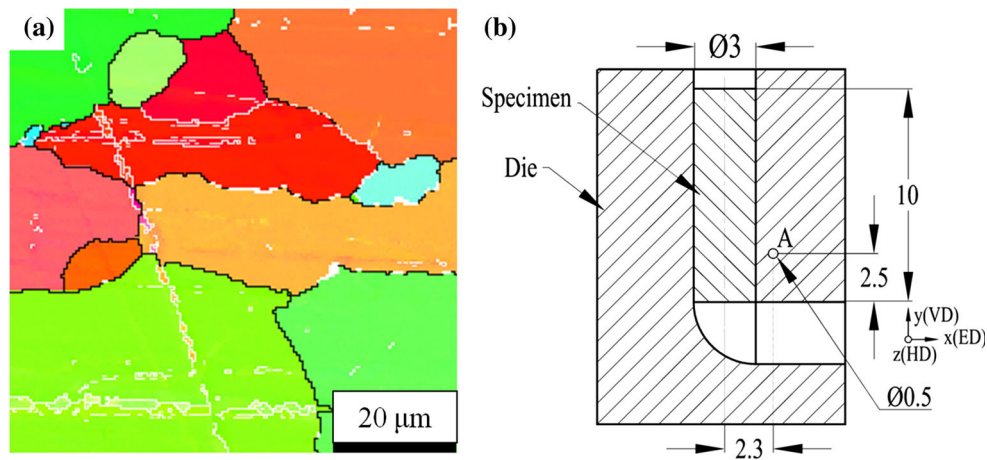
1. Introduction

Grain refinement of Al and its alloys using thermal treatment methods is generally difficult. Because of cross-slip of dislocations caused by their high stacking fault energy (SFE), Al and its alloys exhibit very high rates of dynamic recovery, which is generally expected to completely inhibit dynamic recrystallization (Ref 1, 2). In addition, Al alloys exhibit no phase change during heating. Therefore, ultrafine grains can generally be obtained using severe plastic deformation (SPD) processes.

Equal-channel angular pressing (ECAP) is a SPD process that has received widespread attention because of its simplicity and practicality (Ref 3, 4). ECAP can be used to achieve SPD of materials, reducing grain sizes from the micrometer to nanometer level and resulting in significantly improved strength. Many researchers have applied ECAP and successfully obtained ultrafine-grained Al and its alloys. Iwahashi et al.
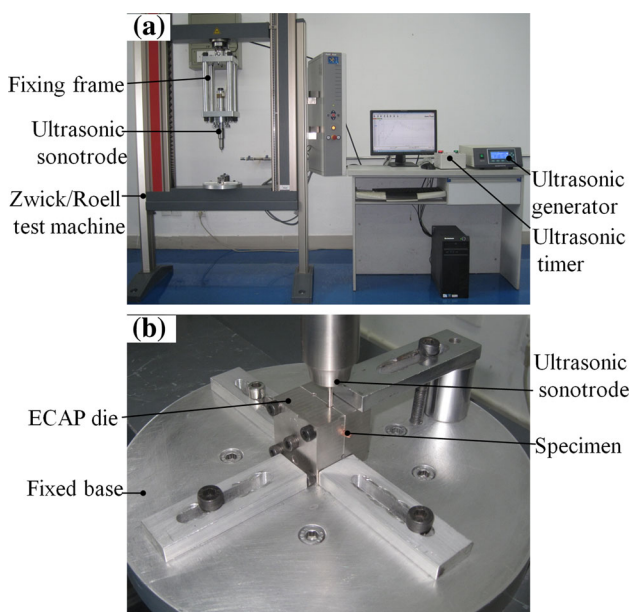
Jianxun Lu, Xiaoyu Wu, Zhaozhi Wu, Zhiyuan Liu, Dengji Guo, and Yan Lou, Guangdong Provincial Key Laboratory of Micro/Nano Optomechatronics Engineering, Shenzhen University, Nan-hai Ave 3688, Shenzhen 518060, Guangdong, People's Republic of China and Shenzhen Key Laboratory of Advanced Manufacturing Technology for Mold&Die, Shenzhen University, Nan-hai Ave 3688, Shenzhen 518060, Guangdong, People's Republic of China; and Shuangchen Ruan, Guangdong Provincial Key Laboratory of Micro/Nano Optomechatronics Engineering, Shenzhen University, Nan-hai Ave 3688, Shenzhen 518060, Guangdong, People's Republic of China. Contact e-mails: wuxy@szu.edu.cn and scruan@szu.edu.cn.

investigated different deformation routes for pure Al, obtaining grain sizes within the range of 0.5-1.5 μm, and showed that rotating the sample by 90° between each pass was optimal for obtaining high-angle grain boundaries (HAGBs) (Ref 5). Additionally, ECAP can be used to optimize material performance in combination with other techniques. Bisadi et al. (Ref 6) combined ECAP and twist extrusion to refine pure Al, which resulted in a more homogeneous strain distribution in the workpieces. However, several issues related to ECAP processing must be overcome. For example, Abib et al. showed that the atomic positions in the typical ECAP-type texture of face-centered cubic (FCC) metals deviated from the ideal positions. The texture did not show any trends toward randomization with increasing pass number (Ref 7). Vaseghi et al. (Ref 8) reported that strain inhomogeneity changed the microstructure of ECAPed Al-6061 and led to inhomogeneity of the mechanical properties throughout the cross section of the final product. Their investigation also revealed that performing ECAP at 100 °C may provide the most homogeneous microstructure. Xu et al. (Ref 9) reported that ultrafine-grained pure Al processed by ECAP showed a strong temperature dependence, with the flow stress decreasing with increasing test temperature. Hasegawa et al. (Ref 10) also investigated the thermal stability of ECAPed Al and its alloys and reported that grains rapidly grew at high temperature. Moreover, excessive extrusion force must be imposed on the material when extruding the material through the ECAP channel.

To address these issues, we propose the use of the intermittent ultrasonic vibration-assisted ECAP (IU-ECAP) technique. IU-ECAP imposes intermittent ultrasonic vibration with the ultrasonic thermal effect controlled by adjusting the intermittent time, whereas other ultrasonic-assisted techniques apply continuous ultrasonic vibration (Ref 11-18), which can lead to overheating and reduce the strength of materials.

Fig. 1 Raw material and extrusion die. (a) Microstructure of as-received bar and (b) schematic and axis reference system of the pressing channel

Fig. 2 Experimental platform: (a) related equipment and (b) main working parts

IU-ECAP has been successfully applied to process ultrafine-grained Cu, resulting in a smaller and more homogeneous structure (Ref 19). In this work, Al-6061 alloy with high SFE is used as the raw material to prepare ultrafine-grained alloys, and the microstructure and mechanical properties of the ultrafine-grained Al-6061 alloy processed using both ECAP and IU-ECAP are compared.

2. Experimental Procedures

The microstructure of Al-6061 alloy bar (0.60% Si, 1.0% Mg, 0.35% Cu, 0.25% Mn, 0.25% Fe, 0.25% Cr, 0.25% Zn, balance Al, mass%) used in this work is shown in Fig. 1(a). The mean grain size of the material was 7 μm in the as-received state. The as-received bar was processed into small specimens of 3 mm diameter and 10 mm length. The specimens were

divided into two groups. Group 1 was processed using conventional ECAP, whereas Group 2 was processed using IU-ECAP. At room temperature, both sets of specimens were extruded for eight passes with rotation of the specimen by 90° in the same direction between each pass, which was denoted route Bc in a previous study (Ref 4).

A schematic of the extrusion die and its *XYZ* coordinate reference system is presented in Fig. 1(b), where *X*, *Y*, and *Z* are the extrusion, vertical, and transverse directions, respectively. Both the internal and external angles of the extrusion channel in the die were 90°, and the die was made of tooling steel (SKD11). A thermocouple fixed in the hole (A) was connected to a temperature measurement system (NI 9213), which could record 100 data points/s. Thus, the temperature changes in the die were strictly monitored.

The experimental platform is shown in Fig. 2(a) and (b) and included a fixing frame, an ultrasonic sonotrode, a tensile machine (Zwick/Roell Z050), a 2-kW ultrasonic generator capable of generating ultrasound at a 20-kHz frequency with an amplitude of 20 μm, an ultrasonic timer, an ECAP die, and a die base. For Group 2, the ultrasonic timer was used to control the ultrasonic vibration time, whereas the ultrasonic generator and timer were shut down during the extrusion of the Group 1 specimens. To prevent softening of the materials, or even melting from the ultrasonic thermal effect, the ultrasonic working cycle time was set at 8 s, which suspended the ultrasonic exposure for 4 s after every 4 s of exposure. MoS_2 lubricant was used during the extrusion process, and the extrusion speed was 0.05 mm/s.

The microstructures of all the specimens were characterized using electron backscattered diffraction (EBSD; Zeiss Sigma 500). The as-received sample and those after the first pass were scanned using a step size of 0.5 μm. The specimens from the other passes were scanned using a step size of 0.1 μm. Misorientations below 2° were excluded from the data statistics.

X-ray diffraction (XRD) measurements were taken with a Bruker D8 Advance diffractometer. The XRD patterns including the peak maximum positions and full width at half maximum (FWHM) values were measured using MDI Jade 6.0 software. Approximate values of the lattice strain and dislocation density were calculated accordingly.

Specimens of both groups were also subjected to tensile test and microhardness measurements. Each specimen was processed

(a)

(b)

(c)
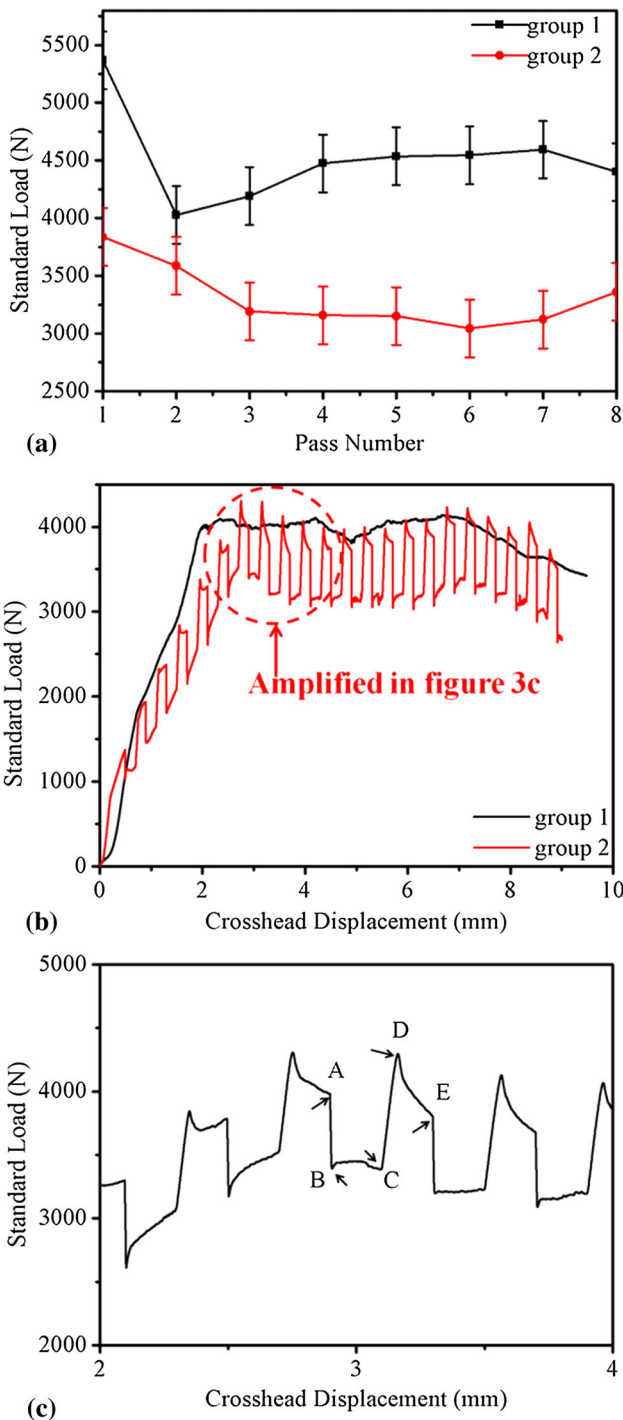
Fig. 3 (a) Extrusion forces of Groups 1 and 2. (b) Load and deformation of Groups 1 and 2 after the eighth pass. (c) Square wave analysis for Group 2

into a standard dog-bone shape with dimensions of $4 \times 1 \times 1$ mm. The crosshead speed of the tensile machine was set at 0.5 mm/min. Microhardness measurements were taken using Vickers indentation with a load of 100 g and loading time of 5 s.

Differential scanning calorimetry (DSC, DSC Q200) and annealing tests were performed to investigate the thermal stability of both groups after the eighth pass. The recrystallization initiation temperature (T_0), peak temperature (T_p), and recrystallization conversion release energy (E_s) were deter-

mined from the DSC curves. Isothermal annealing and isochronal annealing were performed under vacuum conditions. For the isothermal annealing, a temperature of 190 °C was maintained for 15, 30, 60, 90, 120, or 150 min, and for the isochronal annealing, the temperature was maintained for 30 min at 150, 175, 200, 225, 250, 275, 300, or 325 °C. The microhardness of each specimen was measured after annealing.

3. Results and Discussion

3.1 Extrusion Forces

The maximum extrusion forces of the two groups from the first to eighth passes are shown in Fig. 3(a). The maximum extrusion force for Group 1 was 5367 N and occurred during the first pass. The minimum extrusion force was 4028 N and occurred during the second pass, with the force gradually increasing from the second to seventh passes. The extrusion force for Group 2 gradually decreased to 3043 N from the first to sixth passes and increased from the seventh to eighth passes.

The extrusion forces for Group 2 were 28.5, 10.9, 23.8, 29.4, 30.5, 33, 32, and 23.6% less than those for Group 1 from the first to eighth passes, respectively. The ultrasonic vibration greatly decreased the necessary extrusion forces, with the single-pass extrusion force decreasing by 26.5% on average. These results are consistent with those obtained by other researchers. For instance, Huang et al. (Ref 11) reported that ultrasonic vibration reduced the forming force during upsetting and that the reduction in the maximum force could be attributed to the thermal reduction in the coefficient of friction. Djavanroodi et al. (Ref 16) reported a 13% reduction in the average extrusion force when ultrasonic vibration with an amplitude of 2.5 µm was applied during ECAP; in addition, the force was further reduced with increasing vibration amplitude.

The extrusion forces and deformation curves for the specimens of the two groups during the eighth pass are presented in Fig. 3(b). Overall, similar trends are observed for both curves. However, upon closer examination, differences are apparent. The trend of the extrusion force for Group 2 exhibited a square-wave-like pattern. The reason for this trend is that the ultrasonic timer was preset to suspend for 4 s after every 4 s of exposure. Figure 3(c) shows the ultrasonic exposure curve amplified from Fig. 3(b). When the ultrasonic vibration was started, the load rapidly decreased from Point A to Point B and slowly decreased to Point C. The extrusion force of Point B was defined as the extrusion force for Group 2. Ultrasonic vibration took 4 s from Point A to Point C, and the ultrasonic vibration was turned off at Point C; the load increased rapidly to Point D and then slowly to Point E. In summary, the ABC section was generated by ultrasonic exposure and the conventional load, and the CDE section was generated by the conventional load after the ultrasonic exposure was suspended, resulting in the generation of cyclical square waves.

3.2 Temperature Measurements During Extrusion

The die temperatures of Group 1 and Group 2 at three moments during a single extrusion pass are presented in Fig. 4(a) and (b), respectively. For conventional ECAP, the die temperature remained constant at room temperature. However, for IU-ECAP, the die temperature increased in a square-wave-like fashion. At the beginning of the ultrasonic exposure, the

die temperature rapidly increased from Point A to Point B and then slowly increased to Point C. However, the die temperature rapidly decreased from Point C to Point D and then slowly decreased to Point E after the ultrasonic exposure was suspended. The die temperature increased to 63 °C at the end of the extrusion; after that, the die temperature linearly decreased to room temperature. Over this course of the experiment, the die temperature variation was approximately 38 °C.

Based on the die temperature variations in a single pass, the temperature of the specimens could be approximately calculated. In this analysis, the die-absorbed heat was assumed to be the heat discharged by the specimens. Proceeding further, the model was simplified into heat transmission between a specimen and sleeve (see Fig. 4c). The internal and external diameters of the sleeve were 3 and 4.6 mm, respectively, with a height of 10 mm. The heat Q_1 released from the specimens was equal to the heat Q_2 absorbed by the sleeve, as calculated using formulas 1 and 2:

$$Q_1 = C_1 M_1 \Delta T_1, \tag{Eq 1}$$

$$Q_2 = C_2 M_2 \Delta T_2. \tag{Eq 2}$$

Here, C_1 is the specific heat capacity of Al-6061 (883 J/(kg K)), C_2 is the specific heat capacity of SKD11 (442 J/(kg K)), and M_1 and M_2 are the masses of the specimen and sleeve, respectively, which were calculated based on the dimensions shown in Fig. 4(c). ΔT_2 is the temperature change in the sleeve (38 °C), and ΔT_1 refers to the temperature change in the specimen and can be calculated using formula 3:

$$\Delta T_1 = C_2 M_2 \Delta T_2 / (C_1 M_1). \tag{Eq 3}$$

Based on these calculations, the temperature of the specimens was 97 °C at the end of the extrusion. Liu et al. (Ref 12) discovered that continuous ultrasonic vibration-assisted upsetting could increase the temperature to 507 K in tested specimens. Compared with continuous ultrasonic vibration, IU-ECAP greatly reduces the maximum temperature of the specimen, which can reduce grain growth due to overheating.

3.3 Microstructural Characteristics of Extruded Specimens

The microstructures of the specimens for Groups 1 and 2 after the first, second, fourth, sixth, and eighth passes are shown in Fig. 5 and 6, respectively. In the figures, black lines represent the HAGBs, with angles larger than 15°, whereas white lines represent the low-angle grain boundaries (LAGBs), with angles ranging between 2° and 15°. Large and small grains coexisted and were distributed heterogeneously, which is one of the features observed in ultrafine-grained materials prepared by ECAP and has been mentioned by many researchers (Ref 20-22).

The microstructures of the ECAPed specimens are shown in Fig. 5(a), (b), (c), (d), and (e), respectively. After the first, second, and fourth passes, the material exhibited elongated grains with a well-developed subgrain microstructure and few equiaxed grains. However, as observed in Fig. 5(d) and (e), the fraction of equiaxed grains significantly increased after the sixth pass, indicating that the fraction of LAGBs converted into HAGBs increased after the sixth pass.

The microstructures of the IU-ECAPed specimens are shown in Fig. 6(a), (b), (c), (d), and (e). After the first and second passes, elongated grains and many subgrains were observed in the materials, whereas after the fourth pass, as shown in Fig. 6(c), the fraction of equiaxed grains greatly increased, indicating that the fraction of LAGBs converted into HAGBs increased after the fourth pass. Therefore, we may infer that the ultrasonic vibrations accelerated the grain refinement process.

The grain size changes in the two groups as a function of the pass number are shown in Fig. 7(a). The grain size gradually decreased with increasing pass number. After the first, second, fourth, sixth, and eighth passes, the grain sizes for Group 1 were 2.1, 1.2, 0.94, 0.82, and 0.7 μm, respectively, and those
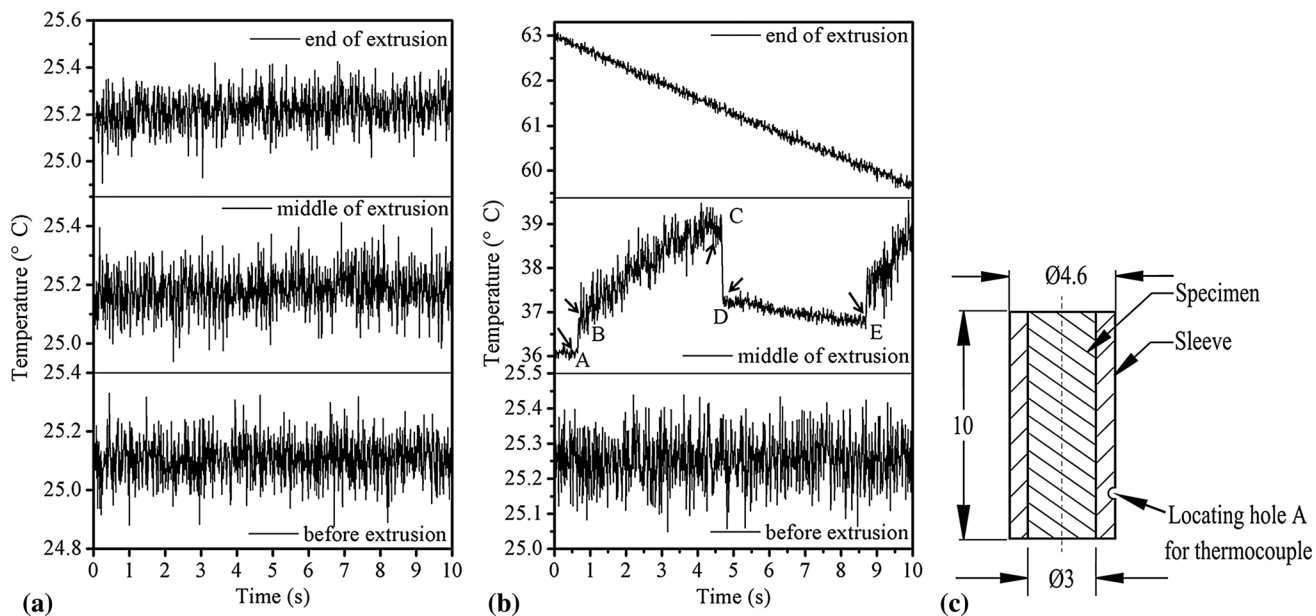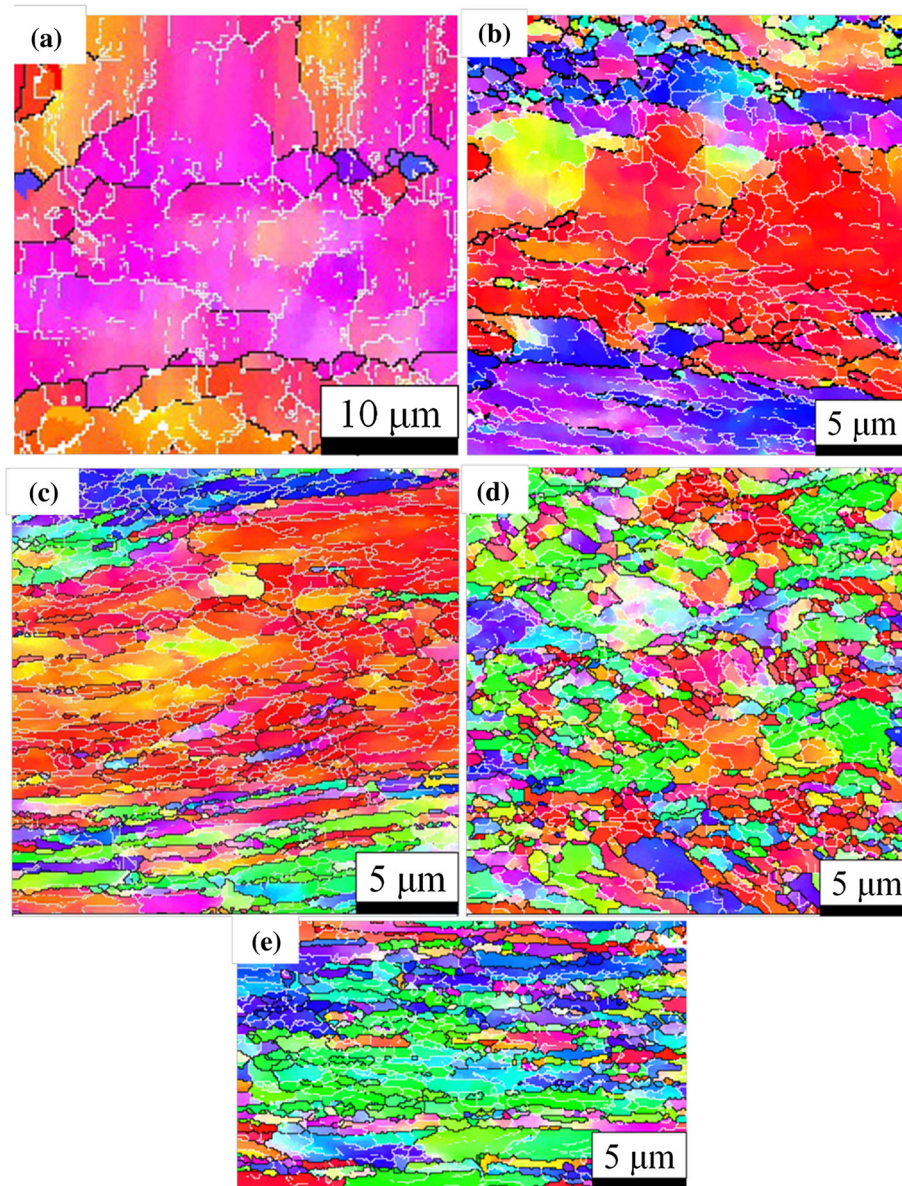

**Fig. 4** Die temperature measurements of (a) Group 1 and (b) Group 2. (c) Simplified die temperature model

Fig. 5 Microstructures of ECAPed specimens after the (a) first, (b) second, (c) fourth, (d) sixth, and (e) eighth passes

for Group 2 were 1.7, 0.95, 0.79, 0.61, and 0.52 μm, respectively. Therefore, the grain sizes of the IU-ECAPed specimens decreased by 23.5, 20.8, 16, 25.6, and 25.7% compared with those of the ECAPed specimens for the first, second, fourth, sixth, and eight passes, respectively. Furthermore, the average grain sizes of Group 1 reached the ultrafine-grain level after the fourth pass; however, no clear decrease in the grain size was observed from the sixth to eighth passes, which may be attributed to the dynamic recovery of the

materials. Because IU-ECAP combines the conventional ECAP with intermittent ultrasonic vibration, larger strain can be produced during the deformation, which greatly accelerates the grain refinement process.

The change in the fraction of HAGBs of the two groups as a function of the pass number is shown in Fig. 7(b). The as-received material exhibited the largest fraction of HAGBs, and the fractions of the HAGBs were the smallest after the first pass. However, after the second, fourth, sixth, and eighth
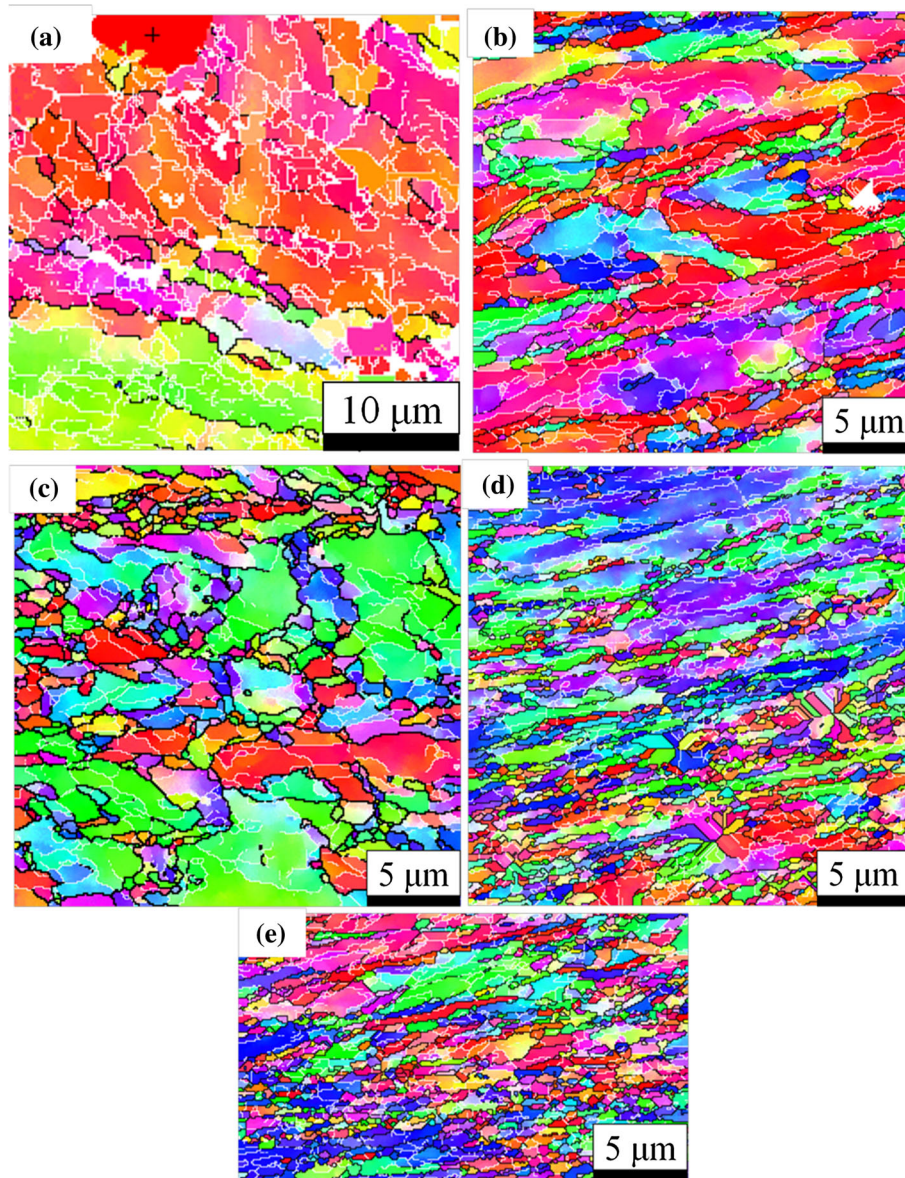
Fig. 6 Microstructures of IU-ECAPed specimens after the (a) first, (b) second, (c) fourth, (d) sixth, and (e) eighth passes

passes, the fraction of HAGBs gradually grew again. The fraction of HAGBs in the IU-ECAPed specimens increased by 6, 17.1, 14.3, 11, and 14.5%, respectively, compared with those of the ECAPed specimens for the first, second, fourth, sixth, and eighth passes. According to the former analysis, only slight changes in die temperature were observed during the ECAP process, whereas the die temperature increased during the IU-ECAP process. Thus, the increasing temperature promoted the conversion of LAGBs to HAGBs.

To further discuss the characteristics of the IU-ECAPed specimens, the grain sizes of the two groups after the eighth pass were determined. As shown in Fig. 7(c), the grain sizes of the ECAPed specimens ranged from 0.15 to 2.0 µm, and two peaks in the grain size distribution were observed. The first peak at 0.45 µm accounted for 10.8% of the distribution, and

the second peak at 1.45 µm accounted for 5.2%. Although the grain sizes of the IU-ECAPed specimens ranged from 0.15 to 1.75 µm, most of the grain sizes were distributed between 0.2 and 1.2 µm; only one peak was located at 0.35 µm, accounting for 8.0% of the distribution. Furthermore, compared with the grains in Fig. 5(b), (c), (d), and (e), the grains in Fig. 6(b), (c), (d), and (e) were dispersed more homogenously for the same pass. We can infer that the grain sizes processed with the ultrasonic vibration were more homogeneous.

3.4 Dislocation Densities of Extruded Specimens

XRD patterns of the as-received bar and Groups 1 and 2 are presented in Fig. 8(a). For the as-received bar, a significant reduction in the intensity of the (1 1 1) fundamental peak
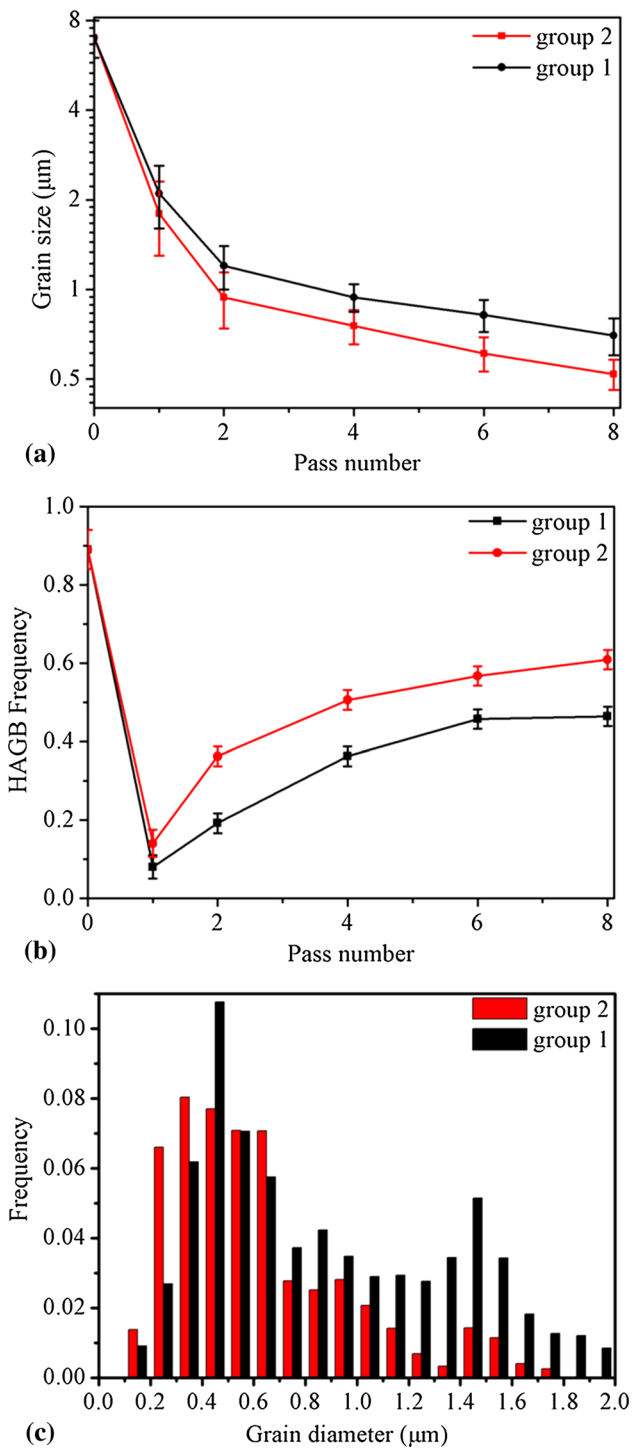
Fig. 7 (a) Grain size and (b) fraction of HAGBs as a function of pass number. (c) Grain sizes of Group 1 and Group 2 after the eighth pass

compared with the other peaks was observed, which indicated textures of the microstructure along the (2 0 0) and (2 2 0) crystal planes. These textures represent the characteristics of annealed Al alloys. For the second pass of Group 1, major reductions in the intensities of the (2 0 0) and (2 2 0) peaks were observed, which indicated that the texture of the ECAPed specimens was along the (1 1 1) crystal plane. Furthermore, for the fourth, sixth, and eighth passes of Group 1, the intensities of

the (1 1 1) peak increased by 22.6, 40, and 43%, respectively, compared with that of the second pass. These results indicate that the intensities of the textures along the (1 1 1) crystal plane increased with increasing pass number for the ECAPed specimens. Other researchers have reported similar results. For instance, Pithan et al. (Ref 23) observed continuous increases in the intensities of the textures of an ECAPed Al-5056 alloy with increasing pass number. In addition, Wang et al. (Ref 24) reported that the textures of an ECAPed Al-2024 alloy developed continuously during extrusion to eight passes. It can thus be concluded that the microstructure of ECAPed Al-6061 scatters heterogeneously because of the texture development. Compared with those for Group 1, the peaks for Group 2 had weaker intensities with larger FWHM values. Although the texture of the IU-ECAPed specimens was along the (1 1 1) crystal plane from the second to eighth passes, the intensities of the textures decreased significantly. Furthermore, for the fourth, sixth, and eighth passes of Group 2, the intensity of the (1 1 1) peak decreased by 35.3, 36.2, and 60.4%, respectively, compared with that of the second pass. This finding may be attributed to the increase in temperature of the IU-ECAPed specimens. Sakai et al. (Ref 25) reported that the structural heterogeneities introduced by SPD generally decrease with increasing temperature. In other words, with the gradually weakened texture, the microstructure of the IU-ECAPed specimens scattered more homogeneously.

Researchers have previously discussed the reasons for XRD peak broadening. Youssef et al. (Ref 26) suggested that the refined grain size and lattice strain could cause XRD peaks to broaden and decrease their intensities. The lattice microstrain can be approximately calculated using FWHM analysis of the XRD line broadening (Ref 27). This investigation presumes that the Cauchy and Gaussian functions can approximate the crystallite size broadening and strain broadening profiles, leading to Eq 4 (Ref 26, 27):

$$\frac{(\delta 2\theta)^2}{\tan^2 \theta_0} = \frac{\lambda}{d}\left(\frac{\delta 2\theta}{\tan \theta_0 \sin \theta_0}\right) + 25\langle e^2 \rangle. \quad \text{(Eq 4)}$$

Here, $\delta 2\theta$ represents the FWHM, θ_0 represents the peak maximum position, λ represents the wavelength, d represents the average grain size (note that to reduce the calculation error, previously measured grain sizes were used), and e represents the lattice strain. The lattice strain was calculated by fitting $(\delta 2\theta)^2/\tan^2 \theta_0$ vs. $(\delta 2\theta)/(\tan \theta_0 \sin \theta_0)$ for all the measured peaks of the specimens. The lattice strains of the two groups are shown in Fig. 8(b). Compared with Group 1, Group 2 exhibited a larger lattice strain for the same pass. Moreover, for materials processed by SPD, the dislocation density ρ can be calculated based on d and e, leading to Eq 5 (Ref 28):

$$\rho = 2\sqrt{3}\langle e^2 \rangle^{\frac{1}{2}}/(d \times b). \quad \text{(Eq 5)}$$

Here, b is the Burgers vector and equals $\sqrt{2}a/2$ for an fcc Al alloy. The calculated ρ values of the as-received bar and Group 1 and 2 are presented in Fig. 8(c). The as-received bar had the lowest ρ, and the ρ values of the two groups increased with increasing pass number. The IU-ECAPed specimens had larger ρ values at the same pass. For specimens of Group 1 and 2, the ρ values saturated after the sixth pass, reaching 1.38958 and 2.14926×10^{14} m^{-2}, respectively. XRD analysis indicated that significantly increased ρ values were obtained for the IU-ECAPed specimens.
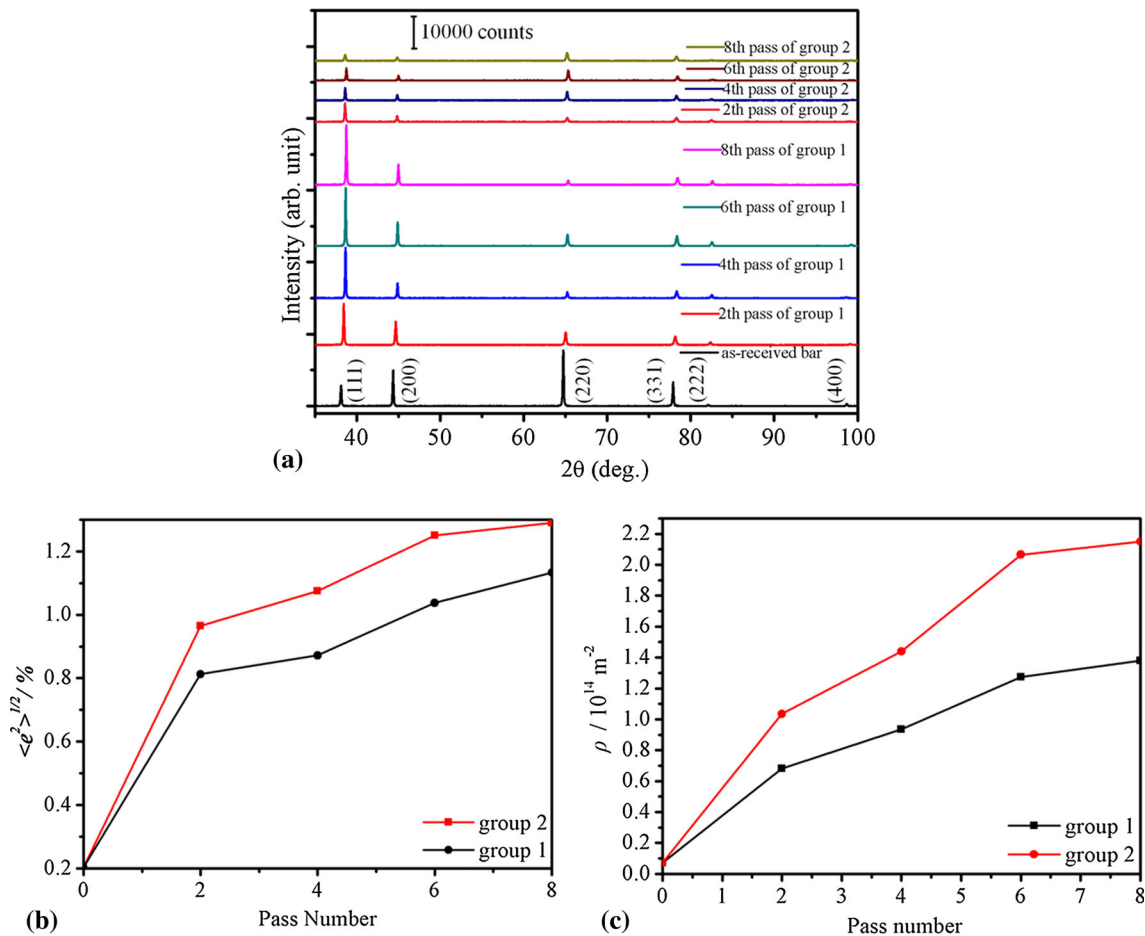
Fig. 8 (a) XRD patterns of as-received bar and Groups 1 and 2. (b) Lattice strain and (c) dislocation densities of Groups 1 and 2

3.5 Mechanical Properties of Extruded Specimens

The ultimate tensile strength (UTS) values of the two groups from the as-received material to the eighth passes are presented in Fig. 9(a). The UTS values of the two groups gradually improved with increasing pass number. The distribution of the error bars indicates that the UTS values of the two groups were saturated after the sixth pass. In addition, the UTS values of Group 2 were larger than those of Group 1 for the same pass. From the first to eighth passes, the UTS values of Group 2 increased by 14.7, 13.4, 10.2, 5.8, 4.8, 4.0, 3.3, and 3.9%, respectively, compared with those of Group 1. Thus, the UTS values for the first four passes showed clear increases, whereas those for the second four passes only showed slight increases.

The microhardness changes in the two groups as a function of pass number are shown in Fig. 9(b). For the ECAPed specimens, the microhardness saturated after the fourth pass, and for the IU-ECAPed specimens, the microhardness saturated after the sixth pass. Moreover, the microhardness of Group 2 was larger than that of Group 1 for the same pass. From the first to eighth passes, the microhardness values of Group 2 were 13.2, 7.6, 7.5, 4.6, 7.2, 9.2, 7.2, and 7.5% larger than those of

Group 1, respectively, and were 8.0% larger on average after each pass.

The strength of a material increases with decreasing grain size according to the Hall–Petch relation (Ref 29, 30):

$$\sigma = \sigma_0 + k_s d^{-1/2}. \tag{Eq 6}$$

Here, σ is the yield stress, σ_0 is the lattice friction stress, and k_s is a yielding constant. To verify the applicability of the Hall–Petch relation, σ was plotted as a function of $d^{-1/2}$, as shown in Fig. 9(c). For Group 1, $\sigma_0 = 225$ MPa and $k_s = 186$ MPa $\mu m^{1/2}$, whereas for Group 2, $\sigma_0 = 253$ MPa and $k_s = 160$ MPa $\mu m^{1/2}$, indicating an increase in σ_0 and decrease in k_s for the IU-ECAPed specimens. The previous analysis revealed that the IU-ECAPed specimens had higher dislocation densities and smaller grain sizes than the ECAPed specimens after the same pass. As a result, the Group 2 specimens had higher UTS and microhardness values than those of Group 1.

3.6 Thermal Stability of Extruded Specimens

The DSC curve for the Group 1 specimens after the eighth pass is shown in Fig. 10(a). The exothermic peak is considered
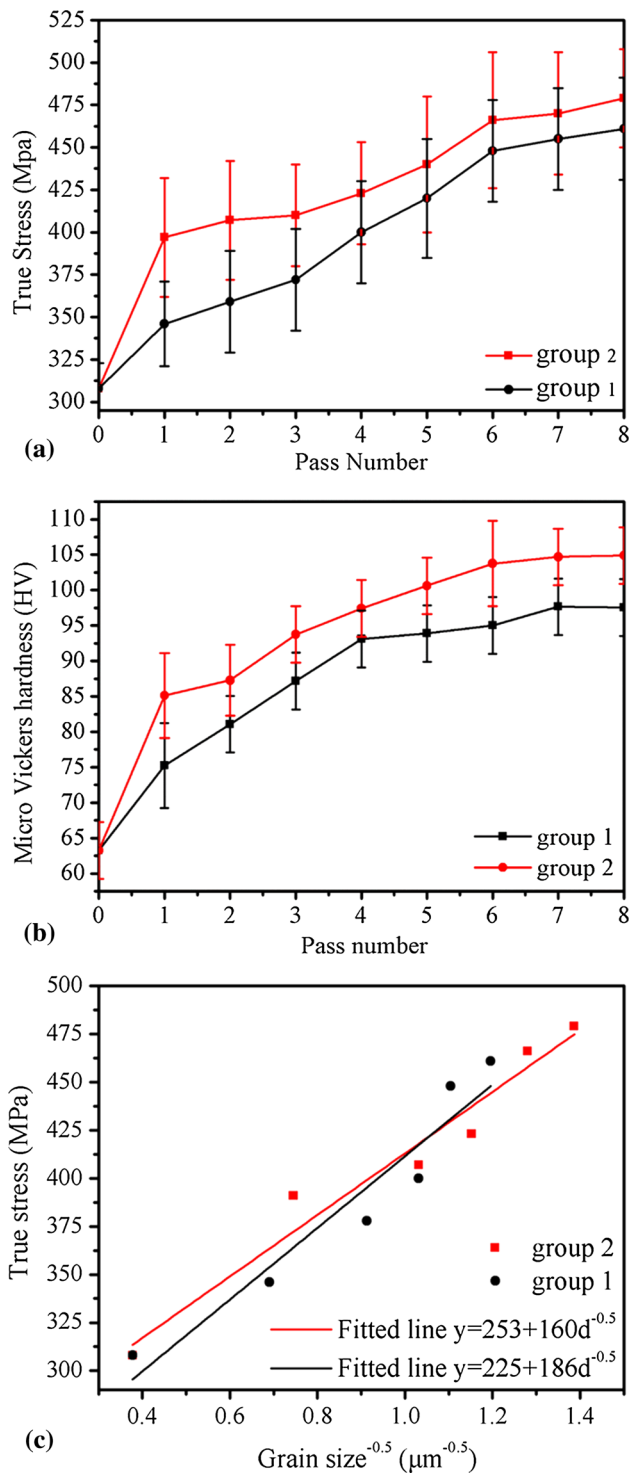
Fig. 9 Mechanical test measurements: (a) true stress of Groups 1 and 2, (b) microhardness as a function of pass number, and (c) Hall–Petch relationship for Groups 1 and 2

to represent the onset of recrystallization (Ref 20), and T_0 was 254 °C, T_p was 258 °C, and E_s was 1.69 J/g. Figure 10(b) presents the DSC curve for the Group 2 specimens after the

eighth pass, showing that T_0 was 330 °C, T_p was 342 °C, and E_s was 2.865 J/g. T_0 and T_p of the IU-ECAPed specimens were 76 and 84 °C higher, respectively, than those of the specimens prepared using conventional ECAP. In addition, the IU-ECAPed specimens released more heat during recrystallization.

The microhardness values of the specimens of the two groups after the eighth pass at different annealing temperatures are presented in Fig. 10(c). The microhardness decreased with increasing temperature. The microhardness of Group 1 decreased from 99.3 to 39 HV from 150 to 250 °C, and the microhardness of Group 2 decreased from 105 to 42 HV from 175 to 325 °C. Figure 10(d) shows the microhardness values of the specimens from the two groups after the eighth pass at 190 °C for different thermal insulation conditions. The two fitted curves in the figures represent recrystallization (Ref 21), and the microhardness values associated with annealing using different thermal insulation times can be obtained from the figure. Compared with Group 2, Group 1 recrystallized faster at 190 °C, and the hardness decreased to 50% of the initial value after 29 min. In contrast, the microhardness of Group 2 decreased to 50% of the initial value after 42 min.

The thermal stability of materials can be defined as a property of the microstructure achieved via SPD that resists recovery and recrystallization (Ref 22). It can be quantitatively evaluated as the time taken for recrystallization to reach 50% in an isothermal annealing experiment or the temperature at which 50% recrystallization is reached for continuous heating or an isochronal experiment. Good thermal stability means that recrystallization occurs at higher temperatures or requires a longer time when materials are heated.

The DSC tests and annealing experiments indicate that the thermal stability of Group 2 was superior to that of Group 1. In addition, the recrystallization temperature determined from the DSC tests was higher than that determined from the annealing experiments, possibly because the thermal insulation of the annealing experiments accelerated recrystallization. Likewise, the absence of thermal insulation in the DSC tests may have postponed recrystallization.

4. Conclusions

This work employed IU-ECAP and ECAP approaches to produce ultrafine-grained Al-6061 alloys, and the differences between the microstructures and mechanical properties of the resultant ultrafine-grained materials were discussed. Compared with conventional ECAP, IU-ECAP has the following advantages:

1. IU-ECAP significantly reduced the necessary extrusion force, with the average extrusion force per pass decreasing by 26.5%.
2. The die temperature exhibited a square-wave-like trend for IU-ECAP during the temperature test, whereas for conventional ECAP, the die temperature remained constant at room temperature. The temperature tests also indicated that the specimen temperature can be adjusted by controlling the intermittent time of IU-ECAP.
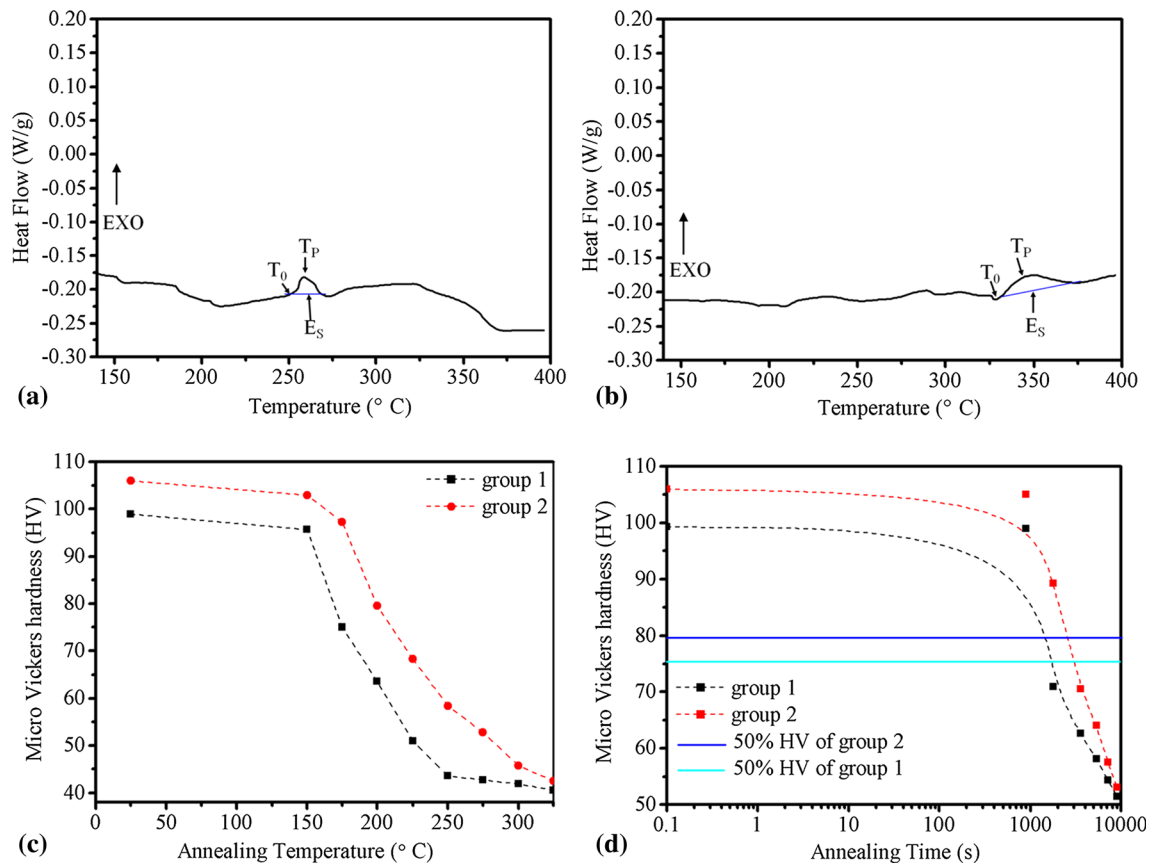
Fig. 10 DSC curves for (a) Group 1 and (b) Group 2 after the eighth pass. Microhardness values after (c) isochronal annealing for 30 min and (d) isothermal annealing at 190 °C

3. IU-ECAP accelerated grain refinement. The resulting ultrafine-grained microstructures were more homogeneous with smaller grain sizes and more HAGBs.
4. Mechanical tests revealed that the UTS and microhardness of the IU-ECAPed specimens were slightly higher than those of the ECAPed specimens after the same pass.
5. XRD analysis indicates that the intensities of the textures for the ECAPed specimens increased with increasing pass number, whereas those for the IU-ECAPed specimens gradually weakened with increasing pass number. These findings suggest that the microstructure of IU-ECAPed specimens scatters more homogeneously. Theoretical calculations indicated that IU-ECAP increases the lattice strain and dislocation densities.
6. DSC and annealing experiments revealed that recrystallization of ultrafine grains processed by IU-ECAP occurs at either a higher temperature or over a longer time. Accordingly, we can infer that ultrafine-grained Al alloys produced by IU-ECAP exhibit better thermal stability.

References

1. S. Gourdet and F. Montheillet, An Experimental Study of the Recrystallization Mechanism During Hot Deformation of Aluminium, *Mater. Sci. Eng. A*, 2000, **283**, p 274–288
2. S. Gourdet and F. Montheillet, A Model of Continuous Dynamic Recrystallization, *Acta Mater.*, 2003, **51**, p 2685–2699
3. V.M. Segal, Materials Processing by Simple Shear, *Mater. Sci. Eng. A*, 1995, **197**, p 157–164
4. R.Z. Valiev and T.G. Langdon, Principles of Equal-Channel Angular Pressing as a Processing Tool for Grain Refinement, *Prog. Mater Sci.*, 2006, **51**, p 881–981
5. Y. Iwahashi, Z. Horita, M. Nemoto, and T.G. Langdon, The Process of Grain Refinement in Equal-Channel Angular Pressing, *Acta Mater.*, 1998, **51**, p 3317–3331
6. H. Bisadi, M.R. Mohamadi, H. Miyanaji, and M. Abdoli, A Modification on ECAP Process by Incorporating Twist Channel, *J. Mater. Eng. Perform.*, 2013, **22**, p 875–881
7. K. Abib, J.A.M. Balanos, B. Alili, and D. Bradai, On the Microstructure and Texture of Cu-Cr-Zr Alloy After Severe Plastic Deformation by ECAP, *Mater. Charact.*, 2015, **112**, p 252–258

8. M. Vaseghi, H.S. Kim, A.K. Taheri, and A. Momeni, Inhomogeneity Through Warm Equal Channel Angular Pressing, *J. Mater. Eng. Perform.*, 2013, **22**, p 1666–1671

9. J. Xu, J. Li, L. Shi, D. Shan, and B. Guo, Effects of Temperature, Strain Rate and Specimen Size on the Deformation Behaviors at Micro/Meso-Scale in Ultrafine-Grained Pure Al, *Mater. Charact.*, 2015, **109**, p 181–188

10. H. Hasegawa, S. Komura, A. Utsunomiya, Z. Horita, M. Furukawa, M. Nemoto, and T.G. Langdon, Thermal Stability of Ultrafine-Grained Aluminum in the Presence of Mg and Zr Additions, *Mater. Sci. Eng. A*, 1999, **265**, p 188–196

11. Z. Huang, M. Lucas, and M.J. Adams, Influence of Ultrasonics on Upsetting of a Model Paste, *Ultrasonics*, 2002, **40**, p 43–48

12. Y. Liu, S. Suslov, Q. Han, L. Hua, and C. Xu, Comparison Between Ultrasonic Vibration-Assisted Upsetting and Conventional Upsetting, *Metall. Mater. Trans. A*, 2013, **44**, p 3232–3244

13. D. Pal and B. Stucker, A Study of Subgrain Formation in Al 3003 H-18 Foils Undergoing Ultrasonic Additive Manufacturing Using a Dislocation Density Based Crystal Plasticity Finite Element Framework, *J. Appl. Phys.*, 2013, **113**, p 203517

14. J.F. Zhang, F.Z. Xuan, and Y.X. Xiang, Dislocation Characterization in Cold Rolled Stainless Steel Using Nonlinear Ultrasonic Techniques: A Comprehensive Model, *E.P.L.*, 2013, **103**, p 68003

15. F. Ahmadi, M. Farzin, M. Meratian, S.M. Loeian, and M.R. Forouzan, Improvement of ECAP Process by Imposing Ultrasonic Vibrations, *Int. J. Adv. Manuf. Technol.*, 2015, **79**, p 503–512

16. F. Djavanroodi, H. Ahmadian, K. Koohkan, and R. Naseri, Ultrasonic Assisted-ECAP, *Ultrasonics*, 2013, **53**, p 1089–1096

17. S. Bagherzadeh and K. Abrinia, Effect of Ultrasonic Vibration on Compression Behavior and Microstructural Characteristics of Commercially Pure Aluminum, *J. Mater. Eng. Perform.*, 2015, **24**, p 4364–4376

18. S. Bagherzadeh, K. Abrinia, and Q. Han, Ultrasonic Assisted Equal Channel Angular Extrusion (UAE) as a Novel Hybrid Method for Continuous Production of Ultra-Fine Grained Metals, *Mater. Lett.*, 2016, **169**, p 90–94

19. J.X. Lu, X.Y. Wu, Z.Y. Liu, X.Q. Chen, B. Xu, Z.Z. Wu, and S.C. Ruan, Microstructure and Mechanical Properties of Ultrafine-Grained Copper Produced Using Intermittent Ultrasonic-Assisted Equal-Channel Angular Pressing, *Metall. Mater. Trans. A*, 2016, **47**, p 4648–4658

20. N. Lugo, N. Llorca, J.J. Sunol, and J.M. Cabrera, Thermal Stability of Ultrafine Grains Size of Pure Copper Obtained by Equal-Channel Angular Pressing, *J. Mater. Sci.*, 2010, **45**, p 2264–2273

21. F.J. Humphreys and M. Hatherly, *Recrystallization and Related Annealing Phenomena*, 2nd ed., Elsevier, Amsterdam, 2004

22. W.Q. Cao, C.F. Gu, E.V. Pereloma, and C.H.J. Davies, Stored Energy, Vacancies and Thermal Stability of Ultra-Fine Grained Copper, *Mater. Sci. Eng. A*, 2008, **492**, p 74–79

23. C. Pithan, T. Hashimoto, M. Kawazoe, J. Nagahora, and K. Higashi, Microstructure and Texture Evolution in Ecae Processed A5056, *Mater. Sci. Eng. A*, 2000, **280**, p 62–68

24. S.C. Wang, M.J. Starink, N. Gao, C. Xu, and T.G. Langdon, Grain Structure and Texture Development During ECAP of Two Heat-Treatable Al-Based Alloys, *Rev. Adv. Mater.*, 2005, **10**, p 249–255

25. T. Sakai, A. Belyakov, R. Kaibyshev, H. Miura, and J.J. Jonas, Dynamic and Post-Dynamic Recrystallization Under Hot, Cold and Severe Plastic Deformation Conditions, *Prog. Mater Sci.*, 2014, **60**, p 130–207

26. K.M. Youssef, R.O. Scattergood, K.L. Murty, and C.C. Koch, Nanocrystalline Al–Mg Alloy with Ultrahigh Strength and Good Ductility, *Scr. Mater.*, 2006, **54**, p 251–256

27. H.P. Klug and L. Alexander, *X-Ray Diffraction Procedures for Polycrystalline and Amorphous Materials*, Wiley, New York, 1974

28. G.K. Williamson and R.E. Smallman, Dislocation Densities in Some Annealed and Cold-Worked Metals from Measurements on the X-Ray Debye–Scherrer Spectrum, *Philos. Mag.*, 1956, **1**, p 34–36

29. N.J. Petch, The Cleavage Strength of Polycrystals, *J. Iron. Steel. Inst.*, 1963, **174**, p 25–28

30. E.O. Hall, The Deformation and Ageing of Mild Steel: III, Discussion of Results, *Proc. Phys. Soc.*, 1951, **643**, p 747–752